P H Y S I C A L   R E V I E W   L E T T E R S

Nanotemplate with Holes: Ultrathin Alumina on Ni₃Al(111)

M. Schmid,[1] G. Kresse,[2] A. Buchsbaum,[1] E. Napetschnig,[1] S. Gritschneder,[3,*] M. Reichling,[3] and P. Varga[1]

[1]*Institut für Allgemeine Physik, Technische Universität Wien, 1040 Wien, Austria*
[2]*Faculty of Physics and Centre for Computational Materials Science, University of Vienna, 1090 Wien, Austria*
[3]*Fachbereich Physik, Universität Osnabrück, 49076 Osnabrück, Germany*
(Received 19 June 2007; published 9 November 2007)

We have determined the structure of the ultrathin $(\sqrt{67} \times \sqrt{67})R12.2°$ aluminum oxide on Ni₃Al(111) by a combination of scanning tunneling microscopy and density functional theory. In addition to other local defects, the main structural feature of the unit cell is a 0.4-nm-diameter hole reaching down to the metal substrate. Understanding the structure and metal growth on this oxide allows us to use it as a template for growing highly regular arrays of nanoparticles.

In recent years, there has been increased interest in surface structures that can serve as templates for growing regular arrays of clusters or nanoparticles, e.g., for studying the catalytic and magnetic properties of such particles. Structures with slight undulations of the potential energy surface of diffusing adatoms, such as dislocation networks [1] require exact control of growth parameters to grow regular arrays of clusters and limit the size of the clusters grown to one or very few monolayers. A more robust approach would use substrates with a strong modulation of the potential energy surface, where the deposited material does not wet most of the surface and clusters nucleate at special sites only. Three years ago, it was proposed [2] that boron nitride on Rh(111) forms such a structure, where adatoms would nucleate on the substrate in the holes of this "nanomesh," a model that had to be abandoned, however [3]. A surface oxide on Ni₃Al(111) has been recently shown to provide a reliable template for growing well-ordered Pd and PdAu clusters [4,5], but its structure and thus the reason for its suitability as a template were unknown so far, and it was also unclear why most other metals do not grow in such a regular fashion [6,7]. In the current work, we determine the structure of this oxide, with the conclusion that it forms an oxide mesh with small holes where atoms having a weak affinity to the oxide can nucleate. Based on this knowledge, we demonstrate how this oxide can be employed as a versatile template for growing different metals as well-ordered nanoparticles.

The existence of a well-ordered surface oxide on Ni₃Al(111) has been known since the 1990s [8,9]; its unit cell size and orientation is $(\sqrt{67} \times \sqrt{67})R12.2°$ with respect to the 505 pm cell of an ordered Ni₃Al(111) surface [10]. In scanning tunneling microscopy (STM), a "dot" structure with one dot per unit cell can be observed at sample voltages of $V_s \approx 2.2$ V, and a honeycomblike "network" structure with three depressions per unit cell, thereof one at the position of the dot, appears at $V_s \approx 3.1$ V [10,11]. The similarity of various spectroscopic data between the surface oxides on Ni₃Al(111) and

NiAl(110) suggests that both oxides have the same thickness and are composed of the same building blocks [9].

Preparation of the surface oxide on Ni₃Al(111) is more difficult than on NiAl(110) and also depends on the crystal used, possibly on the exact stoichiometry. For obtaining the desired oxide structure, one of the two crystals used had to be conditioned by a large number of sputtering-annealing cycles with annealing temperatures around 730–880 °C, probably leading to depletion of Al in the near-surface region, a procedure not required for the other crystal. Oxidation was done at an oxygen pressure of 3×10^{-8} mbar for 30 minutes at ≈ 720 °C, with postannealing at 780 °C. Depending on the previous treatment of the crystal, we found that the $(\sqrt{67} \times \sqrt{67})R12.2°$ oxide can coexist with a "stripe" phase [12] and sometimes another $(\sqrt{79} \times \sqrt{79})R17°$ phase with threefold or sixfold symmetry. Deposition experiments were done with the sample at room temperature, and the experimental setup for the STM work was the same as in Ref. [13]. For the density functional theory (DFT) calculations, we have used the Vienna *ab initio* simulation package (VASP) [14], employing the projector augmented wave method [15,16] and the generalized gradient approximation [17]. The computational setup for structure determination was a complete $(\sqrt{67} \times \sqrt{67})R12.2°$ unit cell, with two layers of the Ni₃Al(111) substrate having fixed coordinates and 721 atoms in the oxide, which were relaxed until the average residual forces were 0.01 eV/Å (1257 atoms in total, Γ-only sampling, 280 eV cutoff, ≈ 300 relaxation steps). Unless otherwise noted, calculations for additional metal atoms were done using smaller cells (≈ 250 atoms), without relaxation of the oxide, which was found to be rather stiff.

Figure 1 shows a high-resolution STM image of the $(\sqrt{67} \times \sqrt{67})R12.2°$ structure, revealing sixfold rotational symmetry (two-dimensional space group $p6$), with flower-like features at the sixfold axes. We observe areas with square and triangular arrangement of atoms, reminding us of the surface oxygen (O_s) layer of the ultrathin alumina film on NiAl(110) [13] imaged by STM at similar tunnel-
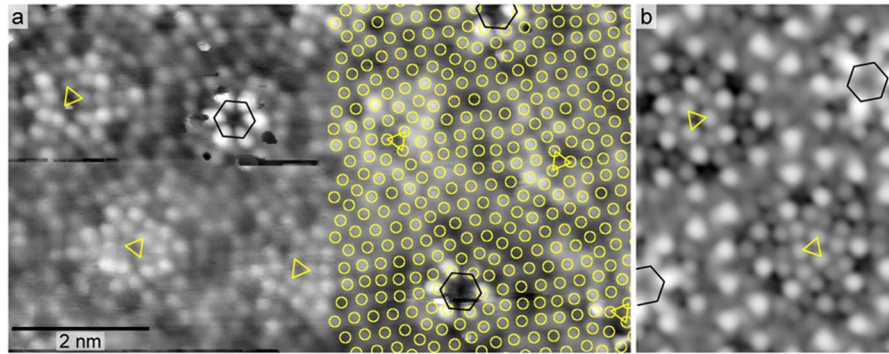
FIG. 1 (color online).   (a) Room-temperature STM image ($V_{\mathrm{sample}} = 58$ mV, $I_t = 35$ nA; 10 nm wide) of the surface oxide. Calculated positions of the O_s atoms are superimposed in the right part of the image. (b) Calculated STM image for voltages near the Fermi level [22]. Threefold and sixfold rotation axes of the oxide are marked by triangles and hexagons, respectively.

ing resistance. This confirms that the two films are structurally similar, and thus the expected stacking sequence is Al-O-Al-O, with the two surface layers (named Al_s and O_s) being almost coplanar. A hexagonal Al_s lattice as on NiAl(110) fits previous LEED data [9], which have already indicated the presence of a lattice with an interatomic distance of ≈ 302 pm. The rotation of this lattice derived from the LEED pattern [10], 23.1° with respect to the substrate, allows us to place the Al_s atoms between the O_s atoms in a natural way. With the exception of the structure inside the sixfold flowerlike features, this information is sufficient to determine the structure model of the surface O_s and Al_s layers.

Concerning the interface, the building rules found for the oxide on NiAl(110) [13] tell us that the lower O atoms (O_i) are almost exactly below the Al_s atoms, and we only have to determine the sites of the Al_i atoms binding to the substrate. We can assume that the strong chemical ordering of the substrate also forces the uppermost substrate layer to be an ordered lattice with Ni_3Al stoichiometry. The sixfold axis of the surface oxide must coincide with a sixfold axis of the topmost substrate layer, i.e., an Al atom of this layer. Assuming that the apparent height (brightness) of the O_s

atoms in the STM image is an indicator whether there is an Al_i atom below [as on NiAl(110)] leads to a honeycomb Al_i lattice in most of the unit cell, with the Al_i atoms close to fcc or hcp hollow sites of the substrate. We find that the Al_i atoms occupy only hollow sites between Ni atoms and avoid Al neighbors in the substrate, which nicely fits the chemical ordering of the substrate and thus indicates that our approach is correct.

The structure shown in Fig. 2 results from analysis of our STM images as described above and relaxation of the structure by DFT. Apart from distortions and a $\approx 10\%$ larger lattice constant, the honeycomb Al_i lattice and the close-packed hexagonal O_i layer above are the same configuration as the corundum structure (α-Al_2O_3). Exceptions of this building rule are found at the threefold axes, where three Al_6 hexagons are replaced by three pentagons and an Al_3 triangle. The Al_3 triangles are the only sites where an O_i atom binds to 3 Al_i atoms, all other O_i atoms bind to 2 Al_i atoms as in the surface oxide on NiAl(110). At the twofold axes, the Al_i atoms bind to two instead of three O_i atoms. All these deviations from the building rules make it possible that the close-packed O_i and Al_s lattices are rotated by 6.9° with respect to the $[11\bar{2}]$
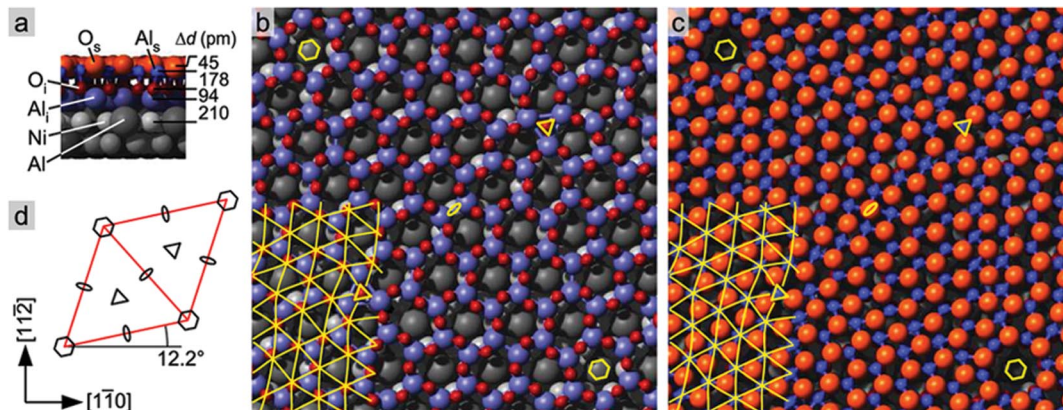

FIG. 2 (color).   The structure obtained by DFT optimization: (a) the side view, (b) the interface, and (c) the surface. The yellow grids in (b) and (c) indicate the distorted hexagonal Al_s lattice, and yellow symbols mark the rotation axes of the unit cell, which is sketched in (d).
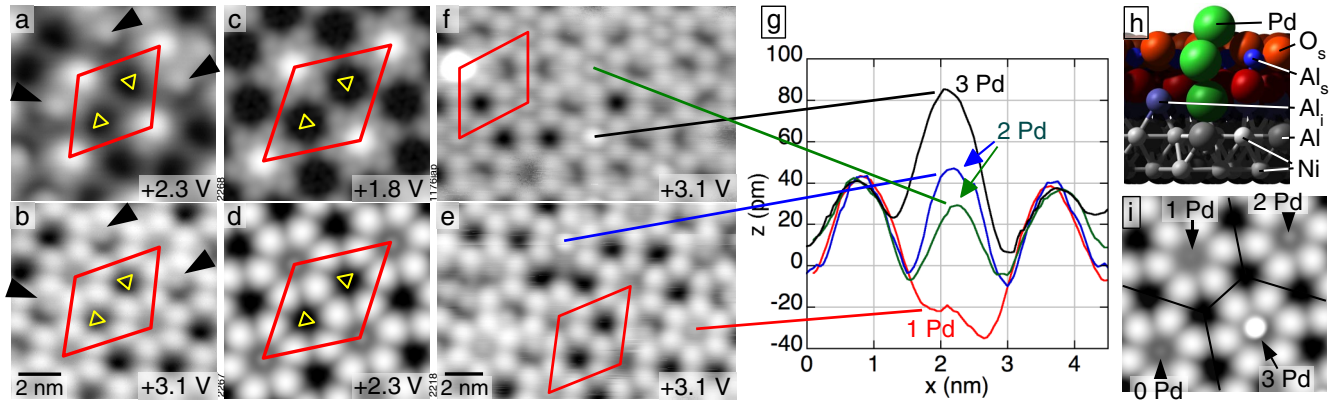
FIG. 3 (color online). Experimental (a), (b) and calculated (c), (d) STM images near the conduction band edge [18]. The unit cell and the threefold rotation axes are indicated. Arrows mark extra defects [21]. (e),(f) Images obtained at +3.1 V after deposition of 0.7 and 3 Pd atoms per unit cell, respectively. The line scans (g) through the unit cell corner are most easily explained by 1, 2, and 3 Pd atoms in the corner hole. (h) Side view of the calculated model with 3 Pd atoms in the corner hole. (i) Mosaic of calculated STM images (+2.3 V) with 0−3 Pd atoms in the corner hole.

direction of the substrate, allowing these atoms to increase their average in-plane distance from 293 pm (the value without rotation) to 302 pm, exactly the same value as on NiAl(110).

What remains to be determined is the structure at the sixfold rotation axis, assumed to be a hole in our model so far (Fig. 2). The STM images do not show any structural features inside the "flowers" composed of 6 O_s atoms, and these flowers always show sixfold symmetry. According to DFT, the oxygen atoms at the edge of the hole have O-O distances of 320 pm; thus, there would be barely enough space for three O atoms and a central Al_s atom inside the hole, a configuration that would break the sixfold symmetry. Indeed, calculated STM images for such an arrangement show that it is incompatible with the symmetry observed, whereas an empty hole at the sixfold axis agrees with the experimental STM images. In neither the simulated nor the experimental images the center of the "flower" appears as dark as one might naively expect for a hole (Fig. 1). Also the appearance of the STM images at higher tunneling voltage is reproduced by the simulation with a hole [Figs. 3(a)−3(d)] [18], identifying the bright dot of the dot structure with the hole. Since STM images near the conduction band edge are sensitive to the local stoichiometry [19], the good agreement between experimental and calculated images also indicates that the structure of the layers not directly visible by STM has been determined correctly.

Our model also explains the hexagonal features observed in a recent noncontact atomic force microscopy (AFM) study [20] (Fig. 4). We find that these dark features correspond to Al_i hexagons and only those hexagons where O_s atoms are directly above the Al_i atoms are observed with good contrast. The contrast observed is the inverse of the geometric heights (O_s atoms in the centers of these hexagons are geometrically low); thus, it must be due to a different mechanism such as different interaction with the

tip or different stiffness of the lattice at these sites. Although the mechanism leading to the AFM image could not be determined so far, the perfect agreement between the features visible in the AFM image with structural entities of the surface oxide provides further support for our model.

As a further test whether the structure at the unit cell corner (i.e., the sixfold axis) is a hole or not, we have deposited small amounts of Pd, corresponding to 0.7 and 3 Pd atoms per oxide unit cell (deposited film thickness 0.0066 and 0.03 Å). It is known that Pd nucleates only at the unit cell corners [4,5]. Comparing section lines through sixfold axes in the STM images [Figs. 3(e)−3(g)] suggests that a single Pd atom per nucleation site (the most frequent configuration at 0.7 atoms/cell) is weakly visible, while at 3 Pd atoms/cell most nucleation sites show a clear protrusion
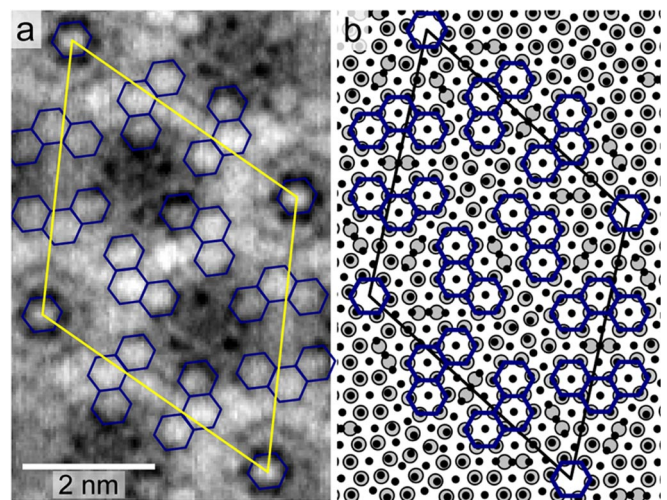

FIG. 4 (color online). (a) AFM image with hexagonal features marked [20]. (b) Structure model showing only the O_s atoms (dots) and Al_i atoms (gray disks). Al_i hexagons with O_s exactly above Al_i are marked.
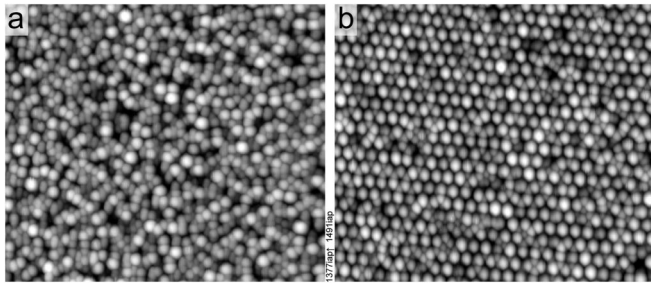
FIG. 5.   STM images (80 nm wide) after deposition of 1 Å Fe (a) without and (b) with predeposition of a 0.03 Å Pd seed layer.

($<$0.1 nm) attributed to 2 or 3 Pd atoms per nucleation site; only a few nucleation sites look like real adatom clusters [height $\gtrsim$ 0.2 nm, e.g., left side of Fig. 3(f)]. This interpretation is in line with DFT calculations showing that up to three Pd atoms fit into the corner hole, with the third Pd atom already 0.16 nm above the O_s layer, but still lower than an adatom on the oxide [Fig. 3(h)]. The simulated STM images [Fig. 3(i)] further support our interpretation, confirming that the first Pd atom appears hardly higher than an empty hole, while 3 Pd atoms appear significantly higher than the oxide [18]. Together with the good agreement between calculated and experimental STM images without Pd, this indicates that the model with a corner hole is correct and one can fit up to 3 Pd atoms into the hole without creating an adatom cluster.

We finally address the question why previous studies [6,7] did not show well-ordered growth of all metals on the oxide nanomesh, even though the corner hole is big enough for any metal atom. Possibly with the exception of the few most reactive ones, metals should wet the substrate in the corner hole much better than the oxygen-terminated oxide surface (DFT calculations for several transition metals show that the adsorption energy in the hole is typically 2 eV larger than on the oxide). Thus it must be difficult for atoms to jump into the holes due to an energy barrier (a kind of Ehrlich-Schwoebel barrier). Indeed, for Fe atoms, a limited set of DFT calculations (for the full cell, including relaxations of the oxide) indicate a barrier $>$0.2 eV, explaining why Fe does not jump into the hole and will eventually nucleate at the second-best site, which is the threefold axis, where the building rules of the oxide are violated. These sites are not all equal due to frequent defects [21], and therefore no well-ordered arrays of clusters are formed [Fig. 5(a)]. Obviously, Pd nucleates in the hole, which nicely agrees with DFT calculations indicating a vanishing barrier for Pd to jump into the hole and a remarkably large capture radius of at least 0.4 nm around the center of the hole. This immediately leads to the possibility of providing a metallic nucleation site by filling the holes with Pd and then depositing another metal. Figure 5(b) shows the result of such an experiment with Fe, where we indeed observe a well-ordered array of Fe

clusters after predeposition of 0.03 Å Pd, i.e., filling the holes with 3 Pd atoms on average. Our results for Co and Pd + Co are similar, and ordered clusters obtained previously for Au deposition with Pd seeds [5] now find an explanation. We expect that many other metals can be grown as well-ordered arrays of clusters by the same method, making this surface oxide a versatile template for highly ordered metallic nanoparticles.

*Present address: Institut für Experimentelle und Angewandte Physik, Universität Regensburg, 93053 Regensburg, Germany.

[1] H. Brune, M. Giovannini, K. Bromann, and K. Kern, Nature (London) **394**, 451 (1998).
[2] M. Corso *et al.*, Science **303**, 217 (2004).
[3] S. Berner *et al.*, Angew. Chem., Int. Ed. **46**, 5115 (2007).
[4] S. Degen, C. Becker, and K. Wandelt, Faraday Discuss. **125**, 343 (2004).
[5] G. Hamm, C. Becker, and C. R. Henry, Nanotechnology **17**, 1943 (2006).
[6] A. Lehnert *et al.*, Surf. Sci. **600**, 1804 (2006).
[7] C. Becker *et al.*, Surf. Sci. **486**, L443 (2001); New J. Phys. **4**, 75 (2002).
[8] U. Bardi, A. Artrei, and G. Rovida, Surf. Sci. **268**, 87 (1992).
[9] C. Becker *et al.*, J. Vac. Sci. Technol. A **16**, 1000 (1998).
[10] S. Degen *et al.*, Surf. Sci. **576**, L57 (2005). Because of the sixfold rotational symmetry of the oxide, the rotation angles of 47.8° given there and 12.2° used here are equivalent.
[11] A. Rosenhahn, J. Schneider, C. Becker, and K. Wandelt, J. Vac. Sci. Technol. A **18**, 1923 (2000).
[12] S. Gritschneder, S. Degen, C. Becker, K. Wandelt, and M. Reichling, Phys. Rev. B **76**, 014123 (2007).
[13] G. Kresse *et al.*, Science **308**, 1440 (2005).
[14] G. Kresse and J. Furthmüller, Comput. Mater. Sci. **6**, 15 (1996).
[15] P. E. Blöchl, Phys. Rev. B **50**, 17953 (1994).
[16] G. Kresse and D. Joubert, Phys. Rev. B **59**, 1758 (1999).
[17] J. P. Perdew *et al.*, Phys. Rev. B **46**, 6671 (1992).
[18] As DFT underestimates the width of the band gap, simulations are for lower tunneling voltages than experiment.
[19] M. Schmid *et al.*, Phys. Rev. Lett. **97**, 046101 (2006).
[20] S. Gritschneder, C. Becker, K. Wandelt, and M. Reichling, J. Am. Chem. Soc. **129**, 4925 (2007).
[21] Apart from the deviations from the building rules of the oxide on NiAl(110) included in our model, the oxide on $Ni_3Al(111)$ frequently exhibits a defect breaking the $p6$ symmetry, visible at tunneling voltages close to the conduction band edge [arrows in Figs. 3(a) and 3(b)]. As we did not find different atomic arrangements in the O_s layer by STM, we consider it most likely that this defect is located in the Al_i layer.
[22] J. Tersoff and D. R. Hamann, Phys. Rev. Lett. **50**, 1998 (1983).